International Journal of Engineering and Geosciences

https://dergipark.org.tr/en/pub/ijeg

e-ISSN 2548-0960

Relationship between land surface temperature and normalized difference water index on various land surfaces: A seasonal analysis

Subhanil Guha[*1] **Himanshu Govil**[1]

[1]*National Institute of Technology Raipur, Department of Applied Geology, Raipur, India*

Keywords
Landsat
Land surface
LST
NDWI
Raipur

ABSTRACT

The present study examines the seasonal relationship between land surface temperature (LST) and normalized difference water index (NDWI) on various land surfaces in Raipur City of India by using a series of Landsat images for four specific seasons since 1991-92. The LST is retrieved using the mono-window algorithm technique. The results show that the LST of the study area is noticeably affected by surface composition. The best correlation (correlation coefficient r = 0.42) between the LST and NDWI is achieved in the post-monsoon season, followed by the monsoon season (r = 0.33), pre-monsoon season (r = 0.25), and winter season (r = 0.04). There is a moderate negative correlation (r = -0.49, -0.33, -0.31, and -0.25 in the pre-monsoon, monsoon, post-monsoon, and winter season, respectively) generated between the LST and NDWI on water bodies. On green vegetation, this LST-NDWI correlation is moderate positive (r = 0.67, 0.43, 0.50, and 0.25 in the pre-monsoon, monsoon, post-monsoon, and winter season, respectively). On human settlement and barren land surface, the correlation is weak positive (r = 0.24, 0.21, 0.27, and 0.15 in the pre-monsoon, monsoon, post-monsoon, and winter season, respectively). The output of the research work can be used in the town planning section of any urban agglomeration.

1. INTRODUCTION

Land surface temperature (LST) is a significant factor for investigating the biogeochemical processes of the land surface (Tomlinson et al. 2011; Hao et al. 2016). A variation on LST is due to the variation in land surface configuration (Hou et al. 2010). Generally, green vegetation and water bodies present low LST, whereas built-up area, bare rock surface or dry soil reflects high LST (Guha et al. 2020a). Thus, LST related studies are very important in urban land use planning and development (Li et al. 2017). Urban heat island and urban hot spots are a very common term in an urban environment and are indicated by the zone of very high LST inside the urban bodies (Guha et al. 2017). Normalized difference water index (NDWI) is the most popular index for water surface extraction and it is invariably used in LULC and LST related studies (McFeeters 1996; Chen et al. 2006; Essa et al. 2012; Yuan et al. 2017; Guha et al. 2020b). Generally, the nature of LST-NDWI relationship in an urban area is insignificant which is controlled by several factors, such as humidity, vegetation, wetland, bare land, air pollution, rock surface, dry or wet soil, heterogeneous man-made materials, etc. (McFeeters 1996; Ghobadi et al. 2014; Guha et al. 2020c).

In many current research articles, the relationship between LST and NDWI was constructed using thermal infrared remote sensing. However, the seasonal analysis of the LST-NDWI relationship in tropical India is rare. The nature of LST and NDWI is changed due to the seasonal changes of evaporation, precipitation, moisture content, air temperature, etc. The LST-NDWI relationship was performed on Raipur City of Chhattisgarh State in Central India as it is not influenced by the humid maritime or dry extreme climatic condition. The study examines the nature and trend of

*Corresponding Author

*(subhanilguha@gmail.com) ORCID ID 0000-0002-2967-7248
(himgeo@gmail.com) ORCID ID 0000-0002-3433-8355

Cite this article

Guha S & Govil H (2021). Relationship between land surface temperature and normalized difference water index on various land surfaces: A seasonal analysis.International Journal of Engineering and Geosciences, 6(3), 165-173

Research Article / DOI: 10.26833/ijeg.821730

Received: 05/11/2020; Accepted: 16/12/2020

the effect of LST on NDWI and the LST-NDWI relation on various land surfaces and their seasonal variation. The main focus of the study is to explore the long-term seasonal analysis of LST-NDWI correlation on various land surfaces. The study will be effective for the future town and country planners for better environmental planning.

2. MATERIALS AND METHOD

2.1. Study area

The Raipur City of India was selected as the study area for the entire research work (Fig. 1). It is the capital and the largest city of Chhattisgarh State of India (URL-1). Raipur is one of the fastest-growing smart cities in India in terms of the urban area and urban population. Fig. 1(a) presents the outline map of India where Chhattisgarh State is located in the middle part (URL-2). Fig. 1(b) presents the outline map of Chhattisgarh State with districts (URL-2). Fig. 1(c) presents the false colour composite (FCC) image of Raipur City from recent Landsat 8 data (Date: 7 November 2018). Fig. 1(d) presents the digital elevation model (Date: 11 October 2011) of Raipur City (URL-3). The total study area extends between 21°11'22"N to 21°20'02"N and 81°32'20"E to 81°41'50"E with an average elevation of 219m to 322m (Fig. 1(d)). The Mahanadi River flows to the east of the city of Raipur, and the southern side has dense forests. The Maikal Hills rise on the northwest of Raipur; on the north, the land rises and merges with the Chota Nagpur Plateau, which extends northeast across Jharkhand state. On the south of Raipur lies the Deccan Plateau. The area is under a tropical wet and dry climate with four typical seasons (pre-monsoon, monsoon, post-monsoon, and winter). Hot and dry pre-monsoon season extends from March to May (Govil et al. 2019). June to September (rainy months) is significantly considered under the monsoon season. October and November months are often considered as the post-monsoon season, characterised by low pollution, moderate temperature, and moderate moisture content in plants and air, and a high percentage of green plants. December to February months (winter season) experience a cool and dry climate. The study area is also characterised by tropical mixed deciduous vegetation and mixed red soil (Govil et al. 2020). The total population of the city is over 1 million, and the sex ratio is 945 (URL-1). The city has an 86.90% total literacy rate (URL-1).

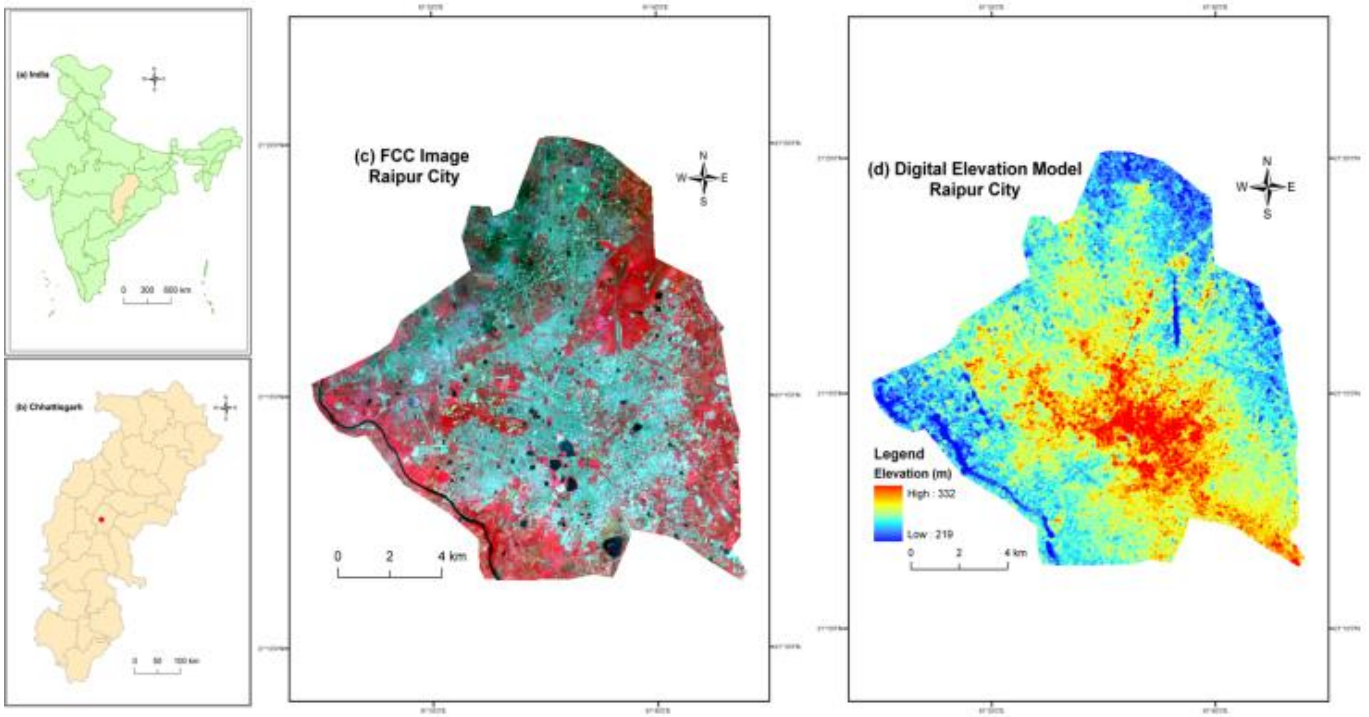

Figure 1. Location of the study area: (a) India (b) Chhattisgarh (c) FCC image of Raipur City (d) DEM of Raipur City

2.2. Data

Table 1 shows the specification of Landsat data of different sensors. Landsat 8 thermal infrared sensors (TIRS) dataset has two TIR bands (bands 10 and 11) in which band 11 has a larger calibration uncertainty. Thus, only TIR band 10 data (100 m resolution) was recommended for the present study (Barsi et al. 2014). Landsat 5 thematic mapper (TM) data has only one TIR band (band 6) of 120 m resolution. Landsat 7 enhanced thematic mapper plus (ETM+) data has a TIR band (band 6) of 60 m resolution. The TIR bands of all the Landsat sensors were resampled to 30 m pixel size by the data provider (URL-3) as the spatial resolution of visible to near-infrared (VNIR) and shortwave infrared (SWIR) bands of the three types of Landsat sensors is 30 m. All the raster calculations were processed in the environment of ArcGIS 9.3 and ERDAS IMAGINE 9.1 software.

Table 1. Specification of Landsat data sets

Date of acquisition	Time (UTC)	Cloud cover (%)	Resolution of TIR bands (m)
18-Mar-91	04:17:34	0	120
03-Apr-91	04:17:46	0	120
21-May-91	04:18:39	1	120
26-Sep-91	04:20:03	13	120
12-Oct-91	04:20:12	6	120
13-Nov-91	04:20:19	1	120
16-Jan-92	04:20:22	3	120
01-Feb-92	04:20:27	0	120
17-Feb-92	04:20:15	4	120
14-Apr-95	04:05:06	0	120
10-Dec-95	03:56:47	0	120
27-Jan-96	04:00:14	0	120
23-Sep-96	04:14:16	2	120
09-Oct-96	04:15:07	0	120
25-Oct-96	04:15:55	5	120
10-Nov-96	04:16:41	7	120
11-Nov-99	04:49:00	0	60
30-Jan-00	04:48:55	0	60
03-Apr-00	04:48:35	0	60
05-May-00	04:48:20	0	60
26-Sep-00	04:46:33	6	60
15-Dec-00	04:46:31	0	60
21-Mar-04	04:35:14	0	120
22-Apr-04	04:36:01	1	120
24-May-04	04:36:54	0	120
09-Jun-04	04:37:23	9	120
29-Sep-04	04:40:16	9	120
15-Oct-04	04:40:36	4	120
16-Nov-04	04:41:11	0	120
02-Dec-04	04:41:33	0	120
18-Dec-04	04:41:52	0	120
19-Jan-05	04:42:17	0	120
04-Feb-05	04:42:29	0	120
03-Mar-09	04:42:22	0	120
19-Mar-09	04:42:44	2	120
04-Apr-09	04:43:05	0	120
20-Apr-09	04:43:24	0	120
06-May-09	04:43:42	0	120
22-May-09	04:44:00	1	120
23-Jun-09	04:44:35	0	120
13-Oct-09	04:46:12	0	120
29-Oct-09	04:46:20	0	120
16-Dec-09	04:46:44	1	120
17-Jan-10	04:46:55	6	120
02-Feb-10	04:46:59	0	120
18-Feb-10	04:47:02	7	100
17-Mar-14	04:56:36	0	100
02-Apr-14	04:56:19	0	100
20-May-14	04:55:38	5	100
05-Jun-14	04:55:45	0	100
12-Nov-14	04:56:21	7	100
30-Dec-14	04:56:09	0	100
15-Jan-15	04:56:09	0	100
31-Jan-15	04:56:04	0	100
16-Feb-15	04:55:55	0	100
12-Mar-18	04:55:43	2	100
28-Mar-18	04:55:36	0	100
15-May-18	04:55:08	0	100
16-Jun-18	04:55:01	2	100
06-Oct-18	04:55:53	0	100
22-Oct-18	04:55:59	0	100
07-Nov-18	04:56:03	0	100
25-Dec-18	04:55:59	0	100
11-Feb-19	04:55:52	0	100
27-Feb-19	04:55:48	4	100

2.3. Retrieving LST from Landsat Data

In this study, the mono-window algorithmwas applied to retrieve LST from multi-temporal Landsat satellite sensors (Qin et al. 2001) where three necessary parameters are ground emissivity, atmospheric transmittance, and effective mean atmospheric temperature. At first, the original TIR bands (100 m resolution for Landsat 8 OLI/TIRS data, 120 m resolution for Landsat 5 TM data, and 60 m resolution for Landsat 7 ETM+ data) were resampled into 30 m by USGS data centre for further application.

The TIR pixel values are firstly converted into radiance from digital number (DN) values (Markham & Barkar 1985). Radiance for TIR band of Landsat 5 TM data and Landsat 7 ETM+ data is obtained using Eq. (1) (URL-3):

$$L_\lambda = \left[\frac{L_{MAX\lambda} - L_{MIN\lambda}}{QCAL_{MAX} - QCAL_{MIN}}\right] * [Q_{CAL} - QCAL_{MIN}] + L_{MIN\lambda} \quad (1)$$

where, L_λ is Top of Atmosphere (TOA) spectral radiance ($Wm^{-2}sr^{-1}mm^{-1}$), Q_{CAL} is the quantized calibrated pixel value in DN, $L_{MIN\lambda}$ ($Wm^{-2}sr^{-1}mm^{-1}$) is the spectral radiance scaled to $QCAL_{MIN}$, $L_{MAX\lambda}$ ($Wm^{-2}sr^{-1}mm^{-1}$) is the spectral radiance scaled to $QCAL_{MAX}$, $QCAL_{MIN}$ is the minimum quantized calibrated pixel value in DN and $QCAL_{MAX}$ is the maximum quantized calibrated pixel value in DN. $L_{MIN\lambda}$, $L_{MAX\lambda}$, $QCAL_{MIN}$, and $QCAL_{MAX}$ values are obtained from the metadata file of Landsat TM and ETM+ data. Radiance for Landsat 8 TIR band is obtained from Eq. (2) (Zanter 2019):

$$L_\lambda = M_L.Q_{CAL} + A_L \quad (2)$$

where, L_λ is the TOA spectral radiance ($Wm^{-2}sr^{-1}mm^{-1}$), M_L is the band-specific multiplicative rescaling factor from the metadata, A_L is the band-specific additive rescaling factor from the metadata, Q_{CAL} is the quantized and calibrated standard product pixel values (DN). All of these variables can be retrieved from the metadata file of Landsat 8 data.

For Landsat 5 and 7 data, the reflectance value is obtained from radiances using Eq. (3) (URL-3):

$$\rho_\lambda = \frac{\pi.L_\lambda.d^2}{ESUN_\lambda.\cos\theta_s} \quad (3)$$

where, ρ_λ is unitless planetary reflectance, L_λ is the TOA spectral radiance ($Wm^{-2}sr^{-1}\mu m^{-1}$), d is Earth-Sun distance in astronomical units, $ESUN_\lambda$ is the mean solar exo-atmospheric spectral irradiances ($Wm^{-2}\mu m^{-1}$) and θ_s is the solar zenith angle in degrees. $ESUN_\lambda$ values for each band of Landsat 5 and 7 can be obtained from the handbooks of the related mission. θ_s and d values can be attained from the metadata file (Coll et al. 2010).

For Landsat 8 data, reflectance conversion can be applied to DN values directly as in Eq. (4) (Zanter 2019):

$$\rho_\lambda = \frac{M_\rho.Q_{CAL} + A_\rho}{\sin\theta_{SE}} \quad (4)$$

where, M_ρ is the band-specific multiplicative rescaling factor from the metadata, A_ρ is the band-specific additive rescaling factor from the metadata, Q_{CAL} is the quantized and calibrated standard product pixel values (DN) and θ_{SE} is the local sun elevation angle from metadata file.

Eq. (5) is used to convert the spectral radiance to at-sensor brightness temperature (Wukelic et al. 1989; Chen et al. 2006):

$$T_b = \frac{K_2}{\ln(\frac{K_1}{L_\lambda}+1)} \quad (5)$$

where, T_b is the brightness temperature in Kelvin (K), L_λ is the spectral radiance in $Wm^{-2}sr^{-1}mm^{-1}$; K_2 and K_1 are calibration constants. For Landsat 8 data, K_1 is 774.89, K_2 is 1321.08 ($Wm^{-2}sr^{-1}mm^{-1}$). For Landsat 7 data, K_1 is 666.09, K_2 is 1282.71 ($Wm^{-2}sr^{-1}mm^{-1}$). For Landsat 5 data, K_1 is 607.76, K_2 is 1260.56 ($Wm^{-2}sr^{-1}mm^{-1}$).

The land surface emissivity ε, is estimated from Eq. (6) using the NDVI Thresholds Method (Sobrino et al. 2001, 2004; Vlassova et al. 2014).

$$\varepsilon = \varepsilon_v F_v + \varepsilon_s(1-F_v) + d\varepsilon \quad (6)$$

where, ε is land surface emissivity, ε_v is vegetation emissivity, ε_s is soil emissivity, F_v is fractional vegetation, $d\varepsilon$ is the effect of the geometrical distribution of the natural surfaces and internal reflections that can be expressed by Eq. (7):

$$d\varepsilon = (1-\varepsilon_s)(1-F_v)F\varepsilon_v \quad (7)$$

where, ε_v is vegetation emissivity, ε_s is soil emissivity, F_v is fractional vegetation, F is a shape factor whose mean is 0.55, the value of $d\varepsilon$ may be 2% for mixed land surfaces Sobrino et al. 2004).

The fractional vegetation F_v, of each pixel, is determined from the NDVI using Eq. (8) (Carlson & Repley 1997):

$$F_v = \left(\frac{NDVI - NDVI_{min}}{NDVI_{max} - NDVI_{min}}\right)^2 \quad (8)$$

where, $(a) NDVI < 0.2$ for bare soil; $(b) NDVI > 0.5$ for vegetation; $(c) 0.2 <= NDVI <= 0.5$ for mixed land with bare soil and vegetation; $(d) NDVI < 0$ for water body (Sobrino et al. 2001, 2004; Vlassova et al. 2014).

Finally, the land surface emissivity ε can be expressed by Eq. (9):

$$\varepsilon = 0.004 * F_v + 0.986 \quad (9)$$

where, ε is land surface emissivity, F_v is fractional vegetation.

Water vapour content is estimated by Eq. (10) (Yang & Qiu 1996; Li 2006):

$$w = 0.0981 * \left[10 * 0.6108 * \exp\left(\frac{17.27*(T_0-273.15)}{237.3+(T_0-273.15)}\right) * RH\right] + 0.1697 \quad (10)$$

where, w is the water vapour content (g/cm^2), T_0 is the near-surface air temperature in Kelvin (K), RH is the relative humidity (%). These parameters of atmospheric profile are the average values of 14 stations around Raipur which are obtained from the Meteorological Centre, Raipur (URL-4) and the Regional Meteorological Centre, Nagpur (URL-5). Atmospheric transmittance is determined for Raipur City using Eq. (11) (Qin et al. 2001; Sun et al. 2010):

$$\tau = 1.031412 - 0.11536w \quad (11)$$

where, τ is the total atmospheric transmittance, w is the water vapour content (g/cm^2).

Raipur City is located in the tropical region. Thus, Eq. (12) is applied to compute the effective mean atmospheric transmittance of Raipur (Qin et al. 2001; Sun et al. 2010):

$$T_a = 17.9769 + 0.91715T_0 \quad (12)$$

LST is retrieved from Landsat 5 TM, Landsat 7 ETM+, and Landsat 8 OLI/TIRS satellite data by using Eq. (13-15) (Qin et al. 2001):

$$T_s = \frac{\left[a(1-C-D)+\left(b(1-C-D)+C+D\right)T_b - DT_a\right]}{C} \quad (13)$$

$$C = \varepsilon\tau \quad (14)$$

$$D = (1-\tau)\left[1+(1-\varepsilon)\tau\right] \quad (15)$$

where, ε is the land surface emissivity, τ is the total atmospheric transmittance, C and D are internal parameters based on atmospheric transmittance and land surface emissivity, T_b is the at-sensor brightness temperature, T_a is the mean atmospheric temperature, T_0 is the near-surface air temperature, T_s is the land surface temperature, $a = -67.355351$, $b = 0.458606$.

2.4. Extraction of Different Types of land surface by Using NDWI

Various land surface biophysical parameters were applied to specify different types of land surface features (Govil et al. 2019, 2020). In this study, special emphasis was given on NDWI (McFeeters 1996, 2013) for determining the relationship with LST. NDWI is determined by the green and NIR bands. For, Landsat 5 TM and Landsat 7 ETM+ data, band 2 is used as the green band and band 4 is used as the NIR band, respectively. For Landsat 8 OLI/TIRS data, band 3 and band 5 are used as the green and NIR bands, respectively (Table 2). The value of NDWI is ranged between −1 and +1. Generally, the negative value of NDWI indicates the built-up area and bare land that

have no water surfaces (Table 2). The dryness increases with the increase of the negativity of NDWI. NDWI value ranges between 0 to 0.3 shows the water bodies (McFeeters 2013), whereas NDWI > 0.3 shows the vegetation with water surfaces (McFeeters 1996, 2013; Chen et al. 2006; Guha et al. 2017). Generally, the post-monsoon images reduce the level of air pollution due to the presence of high moisture content in the air and these images also enhance the greenness of an area. Thus, the post-monsoon images are generally considered for the generation of land use/land cover (LULC) maps. LULC maps were generated using the aforesaid threshold limits of NDWI (McFeeters 1996, 2013; Chen et al. 2006: Guha et al. 2017) and the result was validated by the maximum likelihood classification. The average calculated values of the kappa coefficient and overall accuracy for all the images were 0.87 and 92.14%, respectively.

Table 2. Description of NDWI

Acronym	Description	Formulation	References
NDWI	Normalized difference water index	$\frac{Green - NIR}{Green + NIR}$	McFeeters 1996

3. RESULTS AND DISCUSSION

3.1. Extraction of LULC Types Using NDWI

The total area under different LULC categories was shown in Table 3. Water bodies were the most stable LULC type in the study area. Green vegetation was decreased in a very significant amount (76.80 km^2) from 1991-92 to 2018-19. On the other hand, the built-up area and bare land were increased at a very high rate (78.37 km^2 in 27 years) due to rapid land conversion. In 1991-92, the built-up area and bare land were mainly found in the central part of the Raipur City. The northwest portion of the city was urbanised rapidly from 1991-92 to 2004-05 as the percentage of urban vegetation was declined due to the conversion into built-up areas. After 2004-05, the green areas were reduced at an alarming rate as most of the parts of the city were converted into bare land and built-up area. Only the eastern and the south-western parts were covered by urban vegetation.

Table 3. Total area (km^2) under different types of LULC

Year	Green vegetation	Built-up area and bare land	Water bodies
1991-92	140.38	21.16	2.69
1995-96	130.23	31.72	2.29
1999-00	117.74	44.59	1.89
2004-05	112.41	49.68	2.14
2009-10	90.69	71.59	1.95
2014-15	81.63	81.28	1.32
2018-19	63.58	99.53	1.12

3.2. Characteristics of the Spatial Distribution of LST and NDWI

There is a prominent seasonal variation of different periods that occurred in mean and standard deviation (STD) values of LST (Table 4). The winter season indicates the lowest mean LST values for all the years, whereas the highest mean LST values were found in the pre-monsoon seasons during the entire time. From 1991-92 to 2018-19, the mean LST increased in every season. The post-monsoon season has the mean LST value nearer to the winter season, while monsoon season has a slightly high value of mean LST than the post-monsoon season. The average values of LST and the correlation coefficient of LST and NDWI from 1991-92 to 2018-19 were shown in grey shades inside the Table 4.

Fig. 2 shows the seasonal contrast in the distribution of LST from 1991-92 to 2018-19. The pre-monsoon season has the maximum values of mean LST followed by monsoon, post-monsoon, and winter season. The northwest and southeast parts of the study area exhibit high LST. These parts also have a low percentage of urban vegetation and a high percentage of built-up area and bare land. It shows that the proportion of vegetation has been reduced and the built-up area was increased significantly with time. The Pearson's correlation coefficient (r) values between the LST and NDWI for the entire period were moderate positive to weak negative. The post-monsoon season has the best mean correlation coefficient value (0.42), followed by the monsoon (0.34), pre-monsoon (0.25), and winter (0.04) season.

Table 4. Temporal and seasonal variation of LST values and Pearson's correlation coefficient values of LST-NDWI relationship (significant al 0.05 level).

Season	Year of acquisition	LST (°C) Min.	Max.	Mean	Std.	Correlation coefficients for LST-NDWI relationship
Pre-monsoon	1991-92	23.81	36.27	31.54	1.52	0.13
	1995-96	24.54	41.07	34.64	1.89	0.12
	1999-00	26.36	42.23	36.38	1.93	0.33
	2004-05	26.95	44.07	38.01	2.19	0.29
	2009-10	28.81	46.48	39.60	2.54	0.26
	2014-15	31.93	48.22	41.28	1.75	0.29
	2018-19	33.46	51.11	43.74	1.75	0.35
	Average	27.98	44.21	37.88	1.94	0.25
Monsoon	1991-92	19.87	30.83	25.74	1.41	0.26
	1995-96	21.21	33.01	26.50	1.33	0.36
	1999-00	22.76	35.91	27.81	1.34	0.48
	2004-05	24.17	36.20	31.32	1.33	0.38
	2009-10	25.94	38.38	33.06	2.40	0.31
	2014-15	27.74	40.15	34.87	1.68	0.33
	2018-19	30.59	41.98	37.30	1.13	0.36
	Average	24.61	36.64	30.94	1.52	0.34
Post-monsoon	1991-92	19.72	29.56	24.32	1.72	0.35
	1995-96	20.42	30.33	25.12	1.34	0.45
	1999-00	22.41	33.47	26.84	1.91	0.26
	2004-05	23.03	35.25	28.01	1.71	0.34
	2009-10	24.62	37.91	30.26	1.60	0.47
	2014-15	26.24	38.22	31.68	1.12	0.49
	2018-19	28.92	41.28	33.70	1.34	0.55
	Average	23.62	35.15	28.56	1.53	0.42
Winter	1991-92	18.22	28.33	23.29	1.22	0.05
	1995-96	20.08	28.68	24.40	1.04	-0.03
	1999-00	20.44	32.80	25.21	1.81	-0.08
	2004-05	21.08	33.21	26.47	1.25	-0.03
	2009-10	22.06	34.36	27.98	1.23	0.11
	2014-15	22.80	36.21	28.90	1.39	0.03
	2018-19	24.31	38.36	30.46	1.37	0.21
	Average	21.28	33.14	26.67	1.33	0.57

It is seen from Fig. 2 that in 2018-19, more than 90% of the area in the pre-monsoon season was above 38°C LST. The result is different in the winter season, where no area of the city was above 38°C LST. In 1991-92, almost 90% of the area was below 24°C LST in the

winter season. Monsoon and post-monsoon seasons indicate a moderate range of LST. The mean LST of the study area was gradually increased between 1991-92 and 2018-19. The conversion of other lands into the built-up area and bare land influences a lot on the mean LST of the city. Both the changed and unchanged built-up area and bare land suffer from the increasing trend of LST. These results significantly present the influence of climate shift in Raipur City.

Fig. 3 shows the seasonal variation in the spatial distribution of NDWI from 1991-92 to 2018-19. The high and low NDWI regions were seasonally stable since the 1991-92 sessions. Only the values of NDWI were changed, whereas the overall distributional pattern of NDWI remains almost unchanged. The central part of the city always presents a higher NDWI value. A lower NDWI value is seen throughout the periphery of the city.

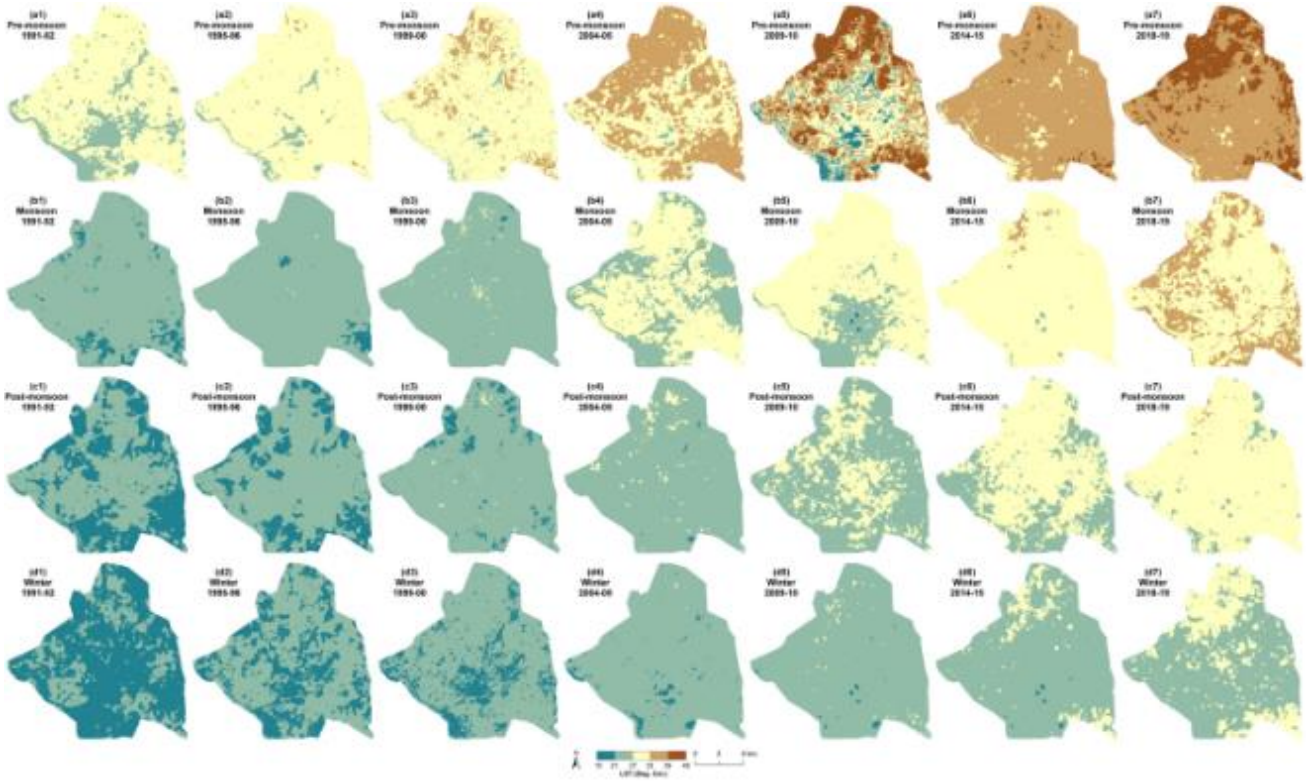

Figure 2. Spatial distribution of LST from 1991-92 to 2018-19: (a1-a7) pre-monsoon season (b1-b7) monsoon season (c1-c7) post-monsoon season (d1-d7) winter season

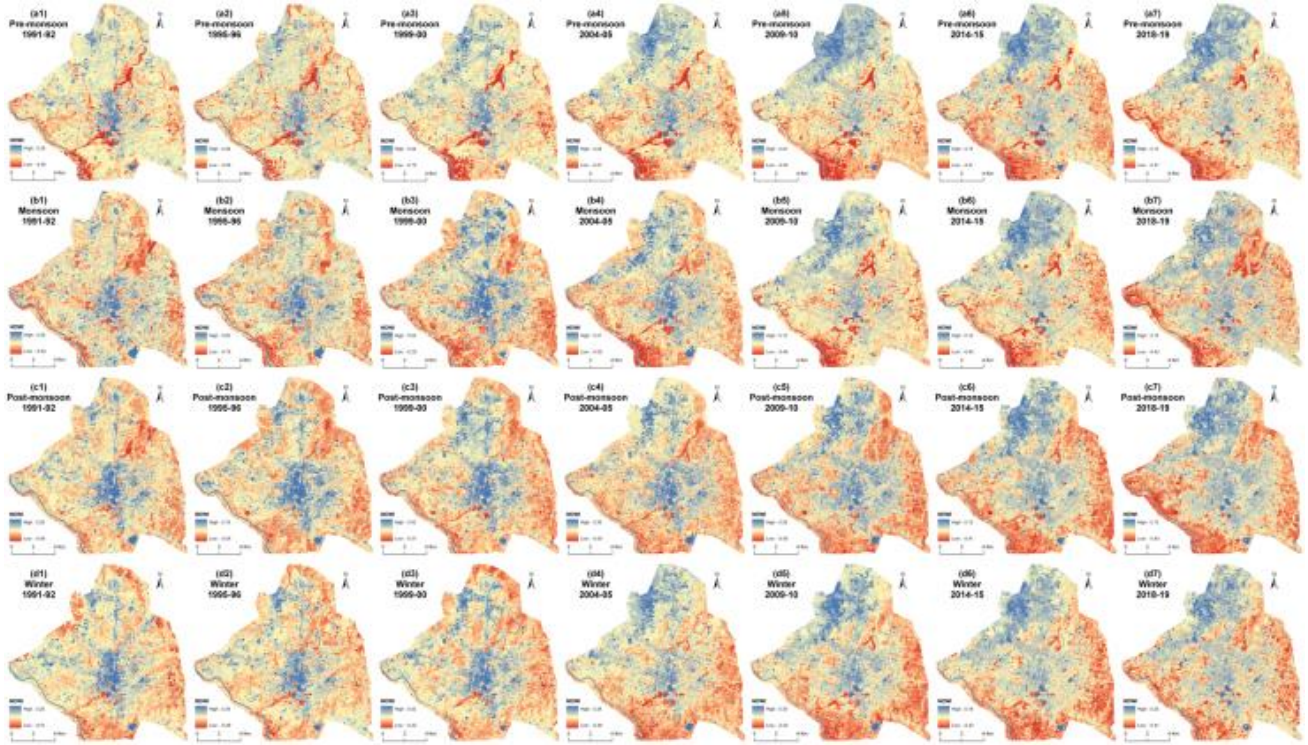

Figure 3. Spatial distribution of NDWI from 1991-92 to 2018-19: (a1-a7) pre-monsoon season (b1-b7) monsoon season (c1-c7) post-monsoon season (d1-d7) winter season

3.3. Relationship between LST and various types of LULC

The LST of the study area significantly depends upon the LULC types. Generally, the area with green vegetation has low LST value; the built-up areas and bare lands have moderate to high LST value, and the water bodies are characterised by a low to moderate range of LST. In the pre-monsoon season, the built-up area and bare land have comparatively high LST than the other LULC types. But in the winter season, these areas have comparatively low to moderate LST due to low emissivity. Green areas and water areas are characterised by a relatively stable range of low LST values.

Fig. 4 presents the temporal changes of LST on various categories of LULC. Vegetation and water surface increases the LST, while bare land/built-up surface decreases LST. Most of the converted lands are built-up or bare land. Consequently, the built-up/bare land surfaces increase, while vegetation and water surface decrease in a significant amount. Land conversion is the main responsible factor for the seasonal change of mean LST. As a result, the mean LST significantly increased (1.60^{o}C in pre-monsoon, 5.34^{o}C in monsoon, 4.76^{o}C in post-monsoon, and 1.08^{o}C in winter season) from 1991-92 to 2018-19.

3.4. Seasonal contrast on LST-NDWI relationship

Table 5 shows the seasonal contrast of LST-NDWI relationships on different LULC types in winter, pre-monsoon, monsoon, and post-monsoon season, respectively. Here, only three types of LULC were considered, i.e., (1) vegetation, (2) water bodies, and (3) built-up area and bare land. On water bodies, the LST-NDWI relationship is moderate negative for any season. NDWI is a water index that is frequently used in water body extraction. On the bare land and built-up area of the study area, the correlation is a weak positive for all four seasons. On green vegetation, the relationship is strong positive (pre-monsoon) to moderate positive (monsoon and post-monsoon), and weak moderate positive (winter). The pre-monsoon season has a strong positive LST-NDWI correlation on the green vegetation (0.67), a weak positive correlation on the bare land and built-up area (0.24), and a moderate negative correlation on green vegetation (-0.49). In the monsoon season, the correlation is moderate positive on green vegetation (0.43), weak positive (0.21) on bare land and built-up area, whereas the correlation is moderate negative (-0.43) on water bodies. The post-monsoon season has a moderate to strong positive correlation (0.50) on green vegetation, a weak positive correlation (0.27) on the bare land and built-up area, and has a moderate negative correlation (-0.31) on water bodies. In winter season, the LST-NDWI correlation is weak positive (0.25) on green vegetation, weak positive (0.15) on built-up area and bare lands. Water bodies have a moderate negative (-0.45) correlation in the winter season.

Fig. 5 represents a generalised view of the overall seasonal variation of LST-NDWI relationships for the whole of the study area. The relationship was positive in the three seasons except for the winter, where it was mostly negative along with some positive values. It can be concluded from Fig. 5 that the post-monsoon season reveals the best correlation, followed by the monsoon and pre-monsoon seasons. There was practically no such relationship found in the winter season. It was mainly due to the high intensity of moisture content in the air. Dry seasons (winter and pre-monsoon) reduce the strength of the correlation, while the wet seasons (post-monsoon and monsoon) enhance the strength of the LST-NDWI correlation.

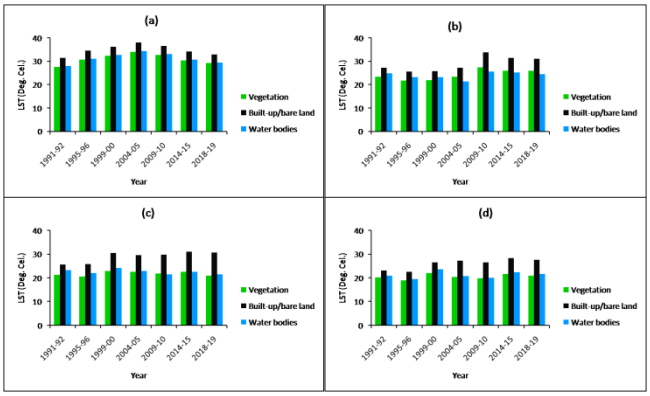

Figure 4. Seasonal variability of mean LST on various categories of LULC: (a) pre-monsoon (b) monsoon (c) post-monsoon (d) winter

Table 5. Seasonal contrast in the LST-NDWI relationship on different types of LULC (significant at 0.05 level).

	Pre-monsoon			Monsoon		
Year	Vegetation	Built-up/bare land	Water bodies	Vegetation	Built-up/bare land	Water bodies
1991-92	0.57	0.08	-0.55	0.23	0.11	-0.41
1995-96	0.60	0.14	-0.49	0.25	0.10	-0.31
1999-00	0.76	0.31	-0.51	0.37	0.29	-0.28
2004-05	0.70	0.14	-0.40	0.33	0.07	-0.35
2009-10	0.73	0.35	-0.46	0.59	0.30	-0.31
2014-15	0.61	0.33	-0.46	0.56	0.34	-0.28
2018-19	0.70	0.35	-0.59	0.65	0.27	-0.42
	0.67	0.24	-0.49	0.43	0.21	-0.33
	Post-monsoon			Winter		
Year	Vegetation	Built-up/bare land	Water bodies	Vegetation	Built-up/bare land	Water bodies
1991-92	0.55	0.19	-0.26	0.39	0.16	-0.49
1995-96	0.57	0.23	-0.22	0.23	0.14	-0.46
1999-00	0.51	0.34	-0.27	0.23	0.10	-0.43
2004-05	0.48	0.28	-0.38	0.19	0.14	-0.55
2009-10	0.49	0.27	-0.45	0.25	0.21	-0.47
2014-15	0.46	0.26	-0.32	0.22	0.11	-0.39
2018-19	0.44	0.32	-0.28	0.26	0.18	-0.34
	0.50	0.27	-0.31	0.25	0.15	-0.45

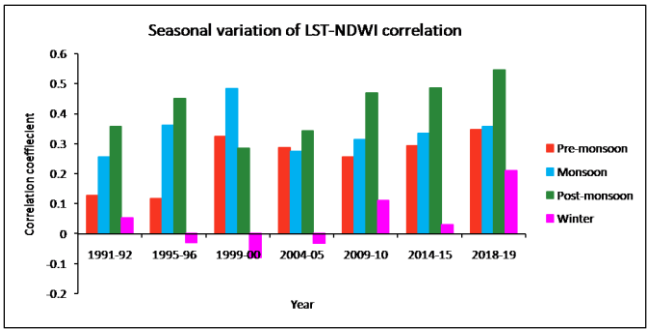

Figure 5. Seasonal contrast on the LST-NDWI relationship for the whole of the study area (significant at 0.05 level)

The present study indicates that LST builds an insignificant correlation with NDWI in Raipur City, India

from 1991-92 to 2018-19 in four different seasons (pre-monsoon, monsoon, post-monsoon, and winter). The result is reliable and significant compared to the other similar studies using Landsat data conducted on the cities from different parts of the world in recent years. NDWI and LST built an insignificant correlation when considering the whole urban area in Wuhan City of China (Wu et al. 2019). Choudhury et al. (2019) showed a negative correlation of the LST-NDWI relationship on the water bodies in the Asansol-Durgapur Development Region, India. LST and NDWI produced a negative correlation on the water bodies of Nanchang City, China (Zhang et al. 2017). A significant negative relationship was found between LST and NDWI on the water bodies in Shenzhen City, China (Chen et al. 2006). The present result shows a significant and stable negative correlation (-0.49, -0.34, -0.31, and -0.45 in pre-monsoon, monsoon, post-monsoon, and winter seasons, respectively) between LST and NDWI on the water bodies throughout the period.

4. CONCLUSION

The present study investigates the temporal and seasonal relationship of LST and NDWI in Raipur City, India using sixty-four Landsat datasets of four different seasons (pre-monsoon, monsoon, post-monsoon, and winter) for 1991-92, 1995-96, 1999-00, 2004-05, 2009-10, 2014-15, and 2018-19. In general, the results show that the relationship between LST and NDWI is insignificant. The correlation is moderate positive in the post-monsoon (0.42) and monsoon (0.34) seasons, whereas it is found weak positive in pre-monsoon (0.25) and winter (0.03). The presence of high moisture content in the air and plants is the main responsible factor for high positivity. The LST-NDWI relationship varies for specific LULC types. The water bodies reflect a moderate negative correlation of LST-NDWI in all the four seasons (-0.49 in pre-monsoon, -0.34 in monsoon, -0.31 in post-monsoon, and -0.45 in winter). On green vegetation, this LST-NDWI correlation is also strong positive in pre-monsoon (0.67), moderate positive in monsoon (0.43) and post-monsoon (0.50), weak positive in winter (0.25). The built-up area and bare land build a weak positive correlation of LST-NDWI in all the four seasons (0.24 in pre-monsoon, 0.21 in monsoon, 0.27 in post-monsoon, and 0.15 in winter). All the four seasons have an insignificant correlation for all LULC types (0.14 in pre-monsoon, 0.10 in monsoon, 0.15 in post-monsoon, and -0.02 in winter). The high percentage of urban vegetation and urban water bodies can promote the ecological health of a rapidly growing city like Raipur. Thus, this research work can be an effective one for the future town and country planners.

ACKNOWLEDGEMENT

The authors are indebted to the United States Geological Survey (URL-3).

REFERENCES

Barsi J, Schott J, Hook S, Raqueno N, Markham B & Radocinski R (2014). Landsat-8 thermal infrared sensor (TIRS) vicarious radiometric calibration. Remote Sensing, 6(11), 11607-11626.

Carlson T N & Ripley D A (1997). On the Relation between NDVI, Fractional Vegetation Cover, and Leaf Area Index. Remote Sensing of Environment, 62, 241-252. https://doi.org/10.1016/S0034-4257(97)00104-1

Chen X L, Zhao H M, Li P X & Yi Z Y (2006). Remote sensing image-based analysis of the relationship between urban heat island and land use/cover changes. Remote Sensing of Environment, 104(2), 133–146. https://doi.org/10.1016/j.rse.2005.11.016

Choudhury D, Das K, & Das A (2019). Assessment of land use land cover changes and its impact on variations of land surface temperature in Asansol-Durgapur Development Region. Egyptian Journal of Remote Sensing and Space Sciences, 22(2), 203-218. https://doi.org/10.1016/j.ejrs.2018.05.004

Coll C, Galve J M, Sanchez J M & Caselles V. 2010. Validation of Landsat-7/ETM+ thermal-band calibration and atmospheric correction with ground-based measurements. IEEE Transactions on Geoscience and Remote Sensing, 48(1), 547–555. https://doi.org/10.1109/TGRS.2009.2024934

Essa W, Verbeiren B, Van der Kwast J, Van de Voorde T & Batelaan O (2012). Evaluation of the DisTrad thermal sharpening methodology for urban areas. International Journal of Applied Earth Observation and Geoinformation, 19, 163-172. https://doi.org/10.1016/j.jag.2012.05.010

Ghobadi Y, Pradhan B, Shafri H Z M & Kabiri K (2014). Assessment of spatial relationship between land surface temperature and land use/cover retrieval from multi-temporal remote sensing data in South Karkheh Sub-basin, Iran. Arabian Journal of Geosciences, 8(1), 525–537. https://doi: 10.1007/s12517-013-1244-3.

Govil H, Guha S, Dey A & Gill N (2019). Seasonal evaluation of downscaled land surface temperature: A case study in a humid tropical city. Heliyon, 5(6), e01923. https://doi.org/ 10.1016/j.heliyon.2019.e01923

Govil H, Guha S, Diwan P, Gill N & Dey A (2020). Analyzing Linear Relationships of LST with NDVI and MNDISI Using Various Resolution Levels of Landsat 8 OLI and TIRS Data. Data Management, Analytics and Innovation. Advances in Intelligent Systems and Computing, 1042. Springer, Singapore, 171-184. https://doi.org/10.1007/978-981-32-9949-8_13

Guha S, Govil H & Besoya M (2020c). An investigation on seasonal variability between LST and NDWI in an urban environment using Landsat satellite data. Geomatics, Natural Hazards and Risk, 11(1), 1319-1345. https://doi.org/10.1080/19475705.2020.1789762

Guha S, Govil H & Mukherjee S (2017). Dynamic analysis and ecological evaluation of urban heat islands in Raipur city, India. Journal of Applied Remote Sensing, 11(3), 036020. https://doi:10.1117/1.JRS.11.036020

Guha S, Govil H, Dey A & Gill N (2020a). A case study on the relationship between land surface temperature and land surface indices in Raipur City, India.

Geografisk Tidsskrift-Danish Journal of Geography, 120(1), 35-50. https://doi.org/10.1080/00167223.2020.1752272

Guha S, Govil H, Gill N & Dey A (2020b). Analytical study on the relationship between land surface temperature and land use/land cover indices. Annals of GIS, 26(2), 201-216. https://doi.org/10.1080/19475683.2020.1754291

Hao X, Li W & Deng H (2016). The oasis effect and summer temperature rise in arid regions-case study in Tarim Basin. Scientific Reports, 6, 35418. https://doi.org/10.1038/srep35418

Hou G L, Zhang H Y, Wang Y Q, Qiao Z H & Zhang Z X (2010). Retrieval and Spatial Distribution of Land Surface Temperature in the Middle Part of Jilin Province Based on MODIS Data. Scientia Geographica sinica, 30, 421-427.

Li J (2006). Estimating land surface temperature from Landsat-5 TM. Remote Sensing Technology and Application, 21, 322-326.

Li W F, Cao Q W, Kun L, & Wu J S (2017). Linking potential heat source and sink to urban heat island: Heterogene-ous effects of landscape pattern on land surface temperature. Science of the Total Environment, 586, 457–465. https://doi.org/10.1016/j.scitotenv.2017.01.191

Markham B L & Barker J K (1985). Spectral characteristics of the LANDSAT thematic mapper sensors. International Journal of Remote Sensing, 6(5), 697–716. https://doi.org/10.1080/01431168508948492

McFeeters S K (1996). The use of the Normalized Difference Water Index (NDWI) in the delineation of open water features. International Journal of Remote Sensing, 17(7), 1425-1432. https://doi.org/10.1080/01431169608948714

McFeeters S K (2013). Using the Normalized Difference Water Index (NDWI) within a Geographic Information System to Detect Swimming Pools for Mosquito Abatement: A Practical Approach. Remote Sensing, 5(7), 3544-3561. https://doi.org/10.3390/rs5073544

Qin Z, Karnieli A & Barliner P (2001). A Mono-Window Algorithm for Retrieving Land Surface Temperature from Landsat TM Data and Its Application to the Israel-Egypt Border Region. International Journal of Remote Sensing, 22(18), 3719-3746. https://doi:10.1080/01431160010006971

Sobrino J A, Jimenez-Munoz J C & Paolini L (2004). Land surface temperature retrieval from Landsat TM5. Remote Sensing of Environment, 9, 434–440. https://doi:10.1016/j.rse.2004.02.003

Sobrino J A, Raissouni N & Li Z (2001). A comparative study of land surface emissivity retrieval from NOAA data. Remote Sensing of Environment, 75(2), 256–266. https://doi.org/10.1016/S0034-4257(00)00171-1

Sun Q, Tan J & Xu Y (2010). An ERDAS image processing method for retrieving LST and describing urban heat evolution: A case study in the Pearl River Delta Region in South China. Environmental Earth Science, 59, 1047-1055.

Tomlinson C J, Chapman L, Trones J E & Baker C (2011). Remote sensing land surface temperature for meteorology and climatology: a review. Meteorological Application, 118, 296–306. https://doi.org/10.1002/met.287

URL-1: https://censusindia.gov.in/2011

URL-2: http://www.surveyofindia.gov.in

URL-3: https://www.earthexplorer.usgs.gov

URL-4: http://www.imdraipur.gov.in

URL-5: http://www.imdnagpur.gov.in

Vlassova L, Perez-Cabello F, Nieto H, Martín P, Riaño D, & De La Riva J (2014). Assessment of methods for land surface temperature retrieval from Landsat-5 TM images applicable to multiscale tree-grass ecosystem modeling. Remote Sensing, 6(5), 4345-4368.

Wu C, Li J, Wang C, Song C, Chen Y, Finka M & Rosa D L (2019). Understanding the relationship between urban blue infrastructure and land surface temperature. Science of the Total Environment, 694, 133742. https://doi.org/10.1016/j.scitotenv.2019.133742

Wukelic G E, Gibbons D E, Martucci L M&Foote H P (1989). Radiometric calibration of Landsat Thematic Mapper thermal band. Remote Sensing of Environment, 28, 339–347. https://doi.org/10.1016/0034-4257(89)90125-9

Yang J & Qiu J (1996). The empirical expressions of the relation between precipitable water and ground water vapor pressure for some areas in China. Scientia Atmospherica Sinica, 20, 620-626.

Yuan X, Wang W, Cui J, Meng F, Kurban A & De Maeyer P (2017). Vegetation changes and land surface feedbacks drive shifts in local temperatures over Central Asia. Scientific Reports, 7(1), 3287. https://doi.org/10.1038/s41598-017-03432-2

Zanter K (2019). Landsat 8 (L8) Data Users Handbook; EROS: Sioux Falls, SD, USA.

Zhang X, Estoque R C & Murayama Y (2017). An urban heat island study in Nanchang City, China based on land surface temperature and social-ecological variables. Sustainable Cities and Society, 32, 557-568. https://doi.org/10.1016/j.scs.2017.05.005